INSTITUT DE FRANCE
Académie des sciences

Comptes Rendus
Mécanique

Vasudevan Kamasamudram and Laurent Stainier

A strain based Lipschitz regularization for materials undergoing damage

Volume 351 (2023), p. 125-149

Published online: 27 March 2023

https://doi.org/10.5802/crmeca.176

Les Comptes Rendus. Mécanique *sont membres du*
Centre Mersenne pour l'édition scientifique ouverte
www.centre-mersenne.org
e-ISSN : 1873-7234

Comptes Rendus
Mécanique
2023, Vol. 351, p. 125-149
https://doi.org/10.5802/crmeca.176

Spontaneous articles / *Articles spontanés*

A strain based Lipschitz regularization for materials undergoing damage

Vasudevan Kamasamudram[*, a] **and Laurent Stainier**[a]

[a] Nantes Université, Ecole Centrale de Nantes, CNRS, GeM, 1 rue de la Noë, 44000 Nantes, France

E-mails: vasudevan.kamasamudram@ec-nantes.fr (V. Kamasamudram), laurent.stainier@ec-nantes.fr (L. Stainier)

Abstract. Data Driven Computational Mechanics (DDCM) solves the boundary value problem by directly relying on the strain-stress data, bypassing the need for a constitutive model. In presence of materials exhibiting a softening response, Finite Element analyses performed with a constitutive model typically use a length scale, which can be introduced into the problem in multiple ways. A few commonly used ways include the addition of the gradient of damage variable in the energy density functional, using the gradient of strain while evaluating the internal variable, and so on. However, in the context of DDCM, these techniques may not be effective as the internal variables are not explicitly defined. Hence, the current article introduces a regularization technique, where the gradient of strain is constrained to lie within some interval. This prevents strain localization within an element by introducing a length scale into the problem. This article demonstrates the effectiveness of such a regularization technique in the case of 1D problems using a constitutive model while comparing its performance with strain gradient (SG) models.

Keywords. Localization, Strain gradient limiter, Regularization, Softening, Damage.

Funding. The authors acknowledge the financial support from ISite NExT at Nantes Université, through IRP project iDDrEAM..

Manuscript received 19 October 2022, revised 13 December 2022 and 25 January 2023, accepted 25 January 2023.

1. Introduction

Local models of damage result in spurious localization of strain and damage in a region that depends on the mesh size. This is a consequence of the lack of a length scale in such models. Different techniques exist in the literature to prevent this mesh dependence and regularize the problem. One of these techniques rely on the gradient of the strain to introduce the length scale onto the problem [1]. In this case, the equivalent strain that is used to evaluate the damage variable is computed using the strain as well as its gradient. This results in the implicit and explicit gradient models. Another approach relies on the computation of a non-local equivalent strain as a weighted integral of the strain variable [2, 3]. In [4], a non-local driving force has been defined

* Corresponding author.

to compute the evolution of the damage variable. On the other hand, the gradient of strain can be included in the stain energy functional directly. The result is the class of strain gradient (*SG*) models, presented in [5,6] and references therein. The introduction of the gradient of the strain in the strain energy functional precludes the localization of strain by introducing a length scale into the model. An analysis of the *SG* models in the presence of damage can be found in [7]. In that study, various cases were considered, where the damage is considered to affect just the elastic (non-gradient) modulus in some cases and both the moduli in some other cases.

The difference between the two approaches in including the *SG* into the analysis is that in the approach by [2], the *SG* is used to compute an effective strain, which in turn affects only the computation of damage. The strain energy density function remains unchanged. This can be seen to be an instance of *uncoupled regularization* with strain regularization in the context of [8]. The *SG* models in [5–7], for instance, include the *SG* in the definition of the strain energy itself. In the latter case, the inclusion of gradient effects affects the solution even during the elastic phase before the material undergoes damage. Also, an analysis performed in [7] reveals that the *SG* models, even though they prevent the localization of damage, result in dissipation that depends on the geometry of the analyzed specimen. In short, for infinitely long specimens, using a *SG* model results in an infinite dissipation.

Other methods of regularizing the problem include introducing the gradient of the damage variable in the strain energy functional, which introduces a characteristic length into the problem [9, 10]. This approach can also be compared to the *Phase Field models*, see for instance [11, 12]. The Thick Level Set method introduced in [13] makes the damage a function of the level set, the zero of which is identified to be the damage front. The norm of the gradient of the level set function is restricted to be equal to 1, which introduces the length scale into the problem. A different approach to introducing non-locality into the model has been introduced in [14, 15]. In [14], the gradient of the damage variable has been constrained to be smaller than (a possibly damage-dependent) value. This prevents the damage from localizing in one element when using a local damage model. In [15], the damage variable is instead constrained to be Lipschitz continuous. This introduces a length scale into the model and prevents the mesh dependence of the solution as in the previous case.

The standard Finite Element techniques obtain the solution of the equations of equilibrium and in this process, a constitutive model is used to describe the behavior of the material. In [16], the material behavior is instead taken to be described by the stress-strain data, ideally obtained from the experiments, thereby eliminating the need for a constitutive model. The methodology is described as *Data Driven Computational Mechanics, DDCM*. The problem is described as obtaining the *mechanical state* - pair of strains and stress, (ϵ, σ), that satisfies the equations of equilibrium and the strain-displacement relations. A *distance* is defined between the mechanical state and the *material states* - the strain-stress data that describes the behavior of the material. In addition to satisfying the equilibrium and compatibility equations, the mechanical states also minimize the distance functional to the set of the material states. An extension of the DDCM to inelastic cases has been performed in [17–19]. In [18, 19], the DDCM has been used to describe the behavior of granular materials and a formulation equivalent to the Cosserat media has been used in [19] to prevent the spurious (shear) strain localization in the numerical simulations.

However, the use of the Cosserat model to regularize the problem requires the presence of shear effects. Hence, they may not be effective in regularizing the spurious localization encountered under mode-I loading (see [1, page 30]) as the rotational degrees of freedom do not become active under such loading. Also, the *internal variables* such as damage typically used in the regularization are not explicitly introduced in DDCM. Hence, the current study intends to introduce the notion of length scale into the problem by modifying the space of displacement functions from where the solution is sought. The search space is modified to include only such functions

whose second gradients are between $-1/\ell_c$ and $1/\ell_c$. In other words, the gradient of strains is restricted to lie in the interval $[-1/\ell_c, 1/\ell_c]$. During the minimization of the strain energy density functional, the second displacement gradients are constrained by using Lagrange multipliers. This can also be interpreted as limiting the energy associated with the gradients of strain to a certain value. This leads to some resemblance of the method presented to the *SG* models.

This article presents the continuum version of the regularization technique where the behavior of the material will be described by a constitutive function. It shall be noted that the intent is to use this methodology with the DDCM, where the FE simulations are performed entirely using the database without any model. Thus, the constitutive model presented in the next section will be replaced by a database of stress-strain pairs. This can be seen as using DDCM for inelastic materials, for instance as in [17], but with the regularization presented in this article. This will be the focus of the future work. Since the regularization is applied on the strains rather than internal variables, the proposed methodology indeed remains valid even in the context of DDCM.

2. The local problem - 1D case

Finding the solution of the boundary value problems consists of minimizing the potential energy functional which is defined as (in the 1D case)

$$\Pi(u) = \int_\Omega \psi(u_{,x})\,\mathrm{d}x - W_{\text{ext}}(u), \tag{1}$$

where $u_{,x}$ denotes the gradient of the displacement, ψ denotes the strain energy functional, and W_{ext} indicates the potential of the external forces. In the case of material that undergoes damage, the strain energy function is made to depend on the damage as well, $\psi(u_{,x}, d)$, where d denotes the damage variable. Damage d takes the values in the interval $[0, 1]$, where the value of 0 indicates a pristine material and 1 indicates a fully damaged material. In this case, the potential energy to be minimized becomes

$$\Pi(u, d) = \int \psi(u_{,x}, d)\,\mathrm{d}x - W_{\text{ext}}(u) + \int_0^t D\,\mathrm{d}t, \tag{2}$$

where D denotes the dissipation function [20]. An evolution equation for damage can be specified using the notion of standard general materials [21].

The dissipation in this case can be written as

$$D = \int_\Omega Y\dot{d}\,\mathrm{d}x, \tag{3}$$

where Y denotes the strain energy release rate, defined as $Y = -\partial\psi/\partial d$. The evolution equation for damage can be written using a positive, one-homogeneous dissipation potential as $\varphi(\dot{d}) = Y_c\dot{d} + \mathbb{1}(\dot{d})$. $\mathbb{1}$ is the indicator function that takes a value of 0 if $\dot{d} \geq 0$ and $+\infty$ otherwise. φ can hence be expressed as

$$\varphi(d^*) = \begin{cases} Y_c d^* & \text{if} \quad d^* \geq 0, \\ +\infty & \text{otherwise.} \end{cases} \tag{4}$$

The above choice of dissipation potential introduces irreversibility of the damage variable. The evolution equation can then be written as

$$Y \in \partial\varphi(\dot{d}). \tag{5}$$

It shall be noted that the subdifferential has been used here as the indicator function is not differentiable. The evolution equation now becomes

$$Y - Y_c \in \partial\mathbb{1}(\dot{d}). \tag{6}$$

This results in the Kuhn–Tucker conditions for the evolution of damage as

$$Y - Y_c = 0 \text{ when } \dot{d} \geq 0, \quad \text{and} \quad Y - Y_c \leq 0 \text{ when } \dot{d} = 0, \tag{7}$$

$$\text{Written compactly, } (Y - Y_c)\dot{d} = 0. \tag{8}$$

When $\dot{d} < 0$, $\partial \mathbb{1}(\dot{d}) = \varnothing$ and hence, $\dot{d} < 0$ is forbidden. Picking a form for the strain energy functional as in [10],

$$\psi(u, d) = \frac{1}{2} g(d) E_0 u_{,x}^2, \tag{9}$$

where $g(d)$ is the *degradation function* which depends on damage and E_0 is the undamaged modulus of the material. It shall be noted that the damage effects do not discriminate between the tensile and compressive loadings in the current formalism as the bar will be subjected to tensile loading only.

The strain energy release rate then becomes

$$Y = -\frac{1}{2} g'(d) E_0 \epsilon^2, \tag{10}$$

where $\epsilon = u_{,x}$ and $'$ denotes the derivative with respect to the argument.

When $\dot{d} = 0$, $Y - Y_c$ should be smaller than 0. This implies

$$|\epsilon| \leq \epsilon_c(d) = \sqrt{-\frac{2Y_c}{E_0 g'(d)}}. \tag{11}$$

The above condition establishes the criterion for the propagation of damage, which depends on the current value of damage. It shall be noted that the function g shall be a monotone decreasing function of damage for the quantity under the square root will be greater than 0 [10].

When $|\epsilon| \geq \epsilon_c$ and $Y = Y_c$, $\dot{d} \geq 0$. This condition can be used to evaluate the damage as

$$d = (g')^{-1}\left(-\frac{2Y_c}{E_0 \epsilon^2}\right), \quad \epsilon \neq 0, \tag{12}$$

such that $d > d_{n-1}$, the damage at the previous time. $\bullet^{-1}$ indicates the inverse of the function $\bullet$ and the damage is obtained by evaluating the inverse at the value of the argument.

Currently, similar to in [10], a *linear damage* model will be used. In this case, g becomes

$$g(d) = \frac{1 - d}{1 + (k - 1)d}. \tag{13}$$

k denotes the ratio of strains when the damage reaches 1 (ϵ_f) and when the damage starts to increase from 0 (ϵ_0), $k = \epsilon_f / \epsilon_0$. Evaluating the derivative and using it in the equation (12),

$$d = \frac{\epsilon - \epsilon_0}{\epsilon_f - \epsilon_0}, \tag{14}$$

subject to $d \geq d_{n-1}$.

It shall be noted that different dissipation and degradation functions (or more generally, stored energy functional) can be used from the ones in this article, for example introducing tension-compression asymmetry. It leads to a perhaps different driving force and damage evolution, but there is no direct effect on the regularization methodology presented.

Remark. It shall be noted that the functional to be minimized can be written as $\Pi(u, d) = \int \left[\psi(u_{,x}, d) + Y_c d\right] \mathrm{d}x - W_{\text{ext}}(u)$, where Y_c can be seen to be energy expended per unit volume for the body to completely undergo damage during homogeneous deformation. Stable solutions are taken to minimize Π with respect to admissible variations of u and d. This is the approach that was followed in [9], where the stability and uniqueness of the solutions for the gradient damage models was investigated.

Limitations

It is well known that the version of the damage model presented is devoid of length scale and as such the uniqueness of the solution is lost when the damage initiates as a consequence of the loss of convexity of the strain energy functional. This manifests itself as the dependence of the solution on the mesh parameter in the Finite Element setting. This can be addressed by multiple approaches. A non-exhaustive list of approaches can be seen as - by using the gradient of damage in the strain energy density functional ([10] and the references therein), by using a non-local version of the driving force as in [4], by using the gradient of the strain when evaluating the damage [2], or by using the strain gradients in the strain energy density functional [5].

An analysis of the *SG* method to introduce the length scale into the model has been carried out in [7]. It was observed in that study that the introduction of strain gradients into the model regularizes the problem. However, it was noted that the energy dissipated during the evolution of damage is dependent on the geometry of the specimen. The damage propagates along the sample till the entire sample is fully damaged. Indeed, for infinitely long specimens, it was observed that the energy dissipated is infinite.

3. The proposed method

The current study proposes to introduce the length scale into the problem by restricting the gradient of strains to lie in a certain range. This prevents the localization of strain in one element and the FE solution is expected to become independent of the mesh parameters. The time interval of interest is discretized as $0 = t_0 < t_1 < t_2 < \cdots < t_f = T$. Starting from the minimization problem as in the previous section, the incremental potential energy at the current time is defined as

$$\Pi(u,d) = \int_\Omega \left[\psi(u_{,x},d) + Y_c d\right] \mathrm{d}x - W_{\text{ext}}(u) + \text{quantities at the previous time.} \tag{15}$$

The *quantities at the previous time* do not affect the minimization process and will be dropped from the definition of Π for convenience. In the usual case, the solution is sought as the pair (u^*, d^*) that minimizes Π, given the damage state, d_{n-1}, at the previous time. The damage variable is taken identically as 0 at $t = 0$.

$$\left(u^*, d^*\right) \in \arg \min_{(u,d)\in\left(\mathscr{C}^u \times \mathscr{C}_n^d; d_{n-1}\right)} \Pi(u,d). \tag{16}$$

Here, $\mathscr{C}^u, \mathscr{C}_n^d$ denote the function spaces of u and d with the appropriate smoothness. They are defined as

$$\mathscr{C}^u = \left\{u \in H^2(\Omega) \,\middle|\, u = u_d \quad \text{on } \partial\Omega_d\right\}, \tag{17}$$

$$\mathscr{C}_n^d = \left\{d \in L^\infty(\Omega) \,\middle|\, d(x) \geq d_{n-1}(x) \quad \text{and} \quad d(x) \in [0,1] \ \forall\, x \in \Omega\right\}, \tag{18}$$

where $H^2(\Omega)$ denotes the space of functions whose second derivatives are square integrable and $L^\infty(\Omega)$ denotes the space of bounded measurable functions in Ω. The irreversibility of damage is thus enforced. The damage is also restricted to lie in the interval $[0,1]$. For convenience, $W(u,d)$ is defined as

$$W(u,d) = \psi(u_{,x},d) + Y_c d, \tag{19}$$

and will be used from hereon.

In the current case, in addition to the regularity requirements on u that arise from the condition $\int \psi(u,d)\,\mathrm{d}x < +\infty$, an additional constraint is added as follows. From the equation (14), it can be seen that the damage depends on the current value of strain. In the models that are devoid of any length scale, the strains and hence the damage tend to localize within one element. This leads to large gradients of damage as well as strain in these regions. Introducing an additional

constraint that *the gradients of strains are bounded by a certain value* on the space from which the displacements are sought is expected to prevent this.

Beginning by defining such a space in 1D case as

$$\mathscr{L} = \left\{ u \in \mathscr{C}^u : \left| u_{,xx} \right| \leq \frac{1}{\ell_c} \right\}. \tag{20}$$

the minimization problem can now be written as

$$\left(u^*, d^*\right) \in \arg \inf_{(u,d) \in \left(\mathscr{C}^u \cap \mathscr{L} \times \mathscr{C}_n^d; d_{n-1}\right)} \Pi(u,d). \tag{21}$$

The constraint on the gradient of strain can be included in the potential energy functional using the indicator function, $\mathbb{1}$, as

$$\Pi(u,d) = \int_\Omega W(u,d)\,\mathrm{d}x - W_{\text{ext}}(u) + \int_{\Omega_c} \mathbb{1}\left\{ \left| u_{,xx} \right| \leq \frac{1}{\ell_c} \right\}(x)\,\mathrm{d}x, \tag{22}$$

where the indicator function is defined as

$$\mathbb{1}\{v \leq a\}(x) = \begin{cases} 0 & \text{if} \quad v(x) \leq a, \\ +\infty & \text{otherwise.} \end{cases} \tag{23}$$

It shall be noted that the constraint is restricted to the region Ω_c, which is defined as

$$\Omega_c = \{ x \in \Omega : d < 1 \}. \tag{24}$$

The constraint is not applied in the regions where the material is fully damaged. The importance of this condition will be made clear in the later sections.

The absolute value in the constraint on the strain gradient in the equation (22) can be removed by expressing it as two constraints: $u_{xx} \leq 1/\ell_c$ and $-u_{xx} \leq 1/\ell_c$. These two constraints can now be applied using the indicator function as

$$\Pi(u,d) = \int_\Omega W(u,d)\,\mathrm{d}x - W_{\text{ext}}(u) + \int_{\Omega_c} \mathbb{1}\left\{ u_{,xx} \leq \frac{1}{\ell_c} \right\}(x)\,\mathrm{d}x + \int_{\Omega_c} \mathbb{1}\left\{ -u_{,xx} \leq \frac{1}{\ell_c} \right\}(x)\,\mathrm{d}x. \tag{25}$$

Clearly, at any point in the body, at most, only one of the above constraints is active. Also, observing that

$$\mathbb{1}\left\{ u_{,xx} \leq \frac{1}{\ell_c} \right\} = \sup_{\lambda \in L^2, \geq 0} \lambda \left(u_{,xx} - \frac{1}{\ell_c} \right), \tag{26}$$

the potential energy can be written as

$$\Pi(u,d) = \int_\Omega W(u,d)\,\mathrm{d}x - W_{\text{ext}}(u) + \sup_{\lambda^+ \in L^2, \geq 0} \int_{\Omega_c} \lambda^+ \left(u_{,xx} - \frac{1}{\ell_c} \right) \mathrm{d}x + \sup_{\lambda^- \in L^2, \geq 0} \int_{\Omega_c} \lambda^- \left(-u_{,xx} - \frac{1}{\ell_c} \right) \mathrm{d}x. \tag{27}$$

By duality, the Lagrange multipliers belong to the space of square integrable functions, $L^2(\Omega)$. The solution now satisfies

$$\left(u^*, d^*\right) \in \arg \inf_{(u,d) \in \left(\mathscr{C}^u, \mathscr{C}_n^d; d_{n-1}\right)} \sup_{\lambda^+, \lambda^+ \in L^2, \geq 0} \Pi^*\left(u, d, \lambda^+, \lambda^-\right), \tag{28}$$

where

$$\Pi^*\left(u, d, \lambda^+, \lambda^-\right) = \int_\Omega W(u,d)\,\mathrm{d}x - W_{\text{ext}}(u) + \int_{\Omega_c} \lambda^+ \left(u_{,xx} - \frac{1}{\ell_c} \right) \mathrm{d}x + \int_{\Omega_c} \lambda^- \left(-u_{,xx} - \frac{1}{\ell_c} \right) \mathrm{d}x.$$

Comparison with the strain gradient models

It shall be noted that both the constraints in the equation (25) cannot be active at the same point and hence, either or both of the λ^+ and λ^- are 0. Defining $\Omega_a \subseteq \Omega_c$ as the region where the Lagrange multipliers are non-zero, the region of integration of the last term can be changed to Ω_a.

Taking the variation of Π^* with respect to u results in

$$\delta^u \Pi^*(u,d,\lambda) = \underbrace{\int_\Omega \sigma \delta u_{,x}\,\mathrm{d}x}_{\delta \mathrm{W}_\sigma} - \delta W_{\mathrm{ext}}(u) + \underbrace{\int_{\Omega_a} \left[\lambda^+ \delta u_{,xx} - \lambda^- \delta u_{,xx}\right] \mathrm{d}x}_{\delta \mathrm{W}_\lambda}. \tag{29}$$

The first integral can be split into integrals in two domains Ω_a and $\Omega \setminus \Omega_a$. Hence,

$$\delta^u \Pi^*(u,d,\lambda) = \int_{\Omega\setminus\Omega_a} \sigma \delta u_{,x}\,\mathrm{d}x + \int_{\Omega_a} \sigma \delta u_{,x}\,\mathrm{d}x - \delta W_{\mathrm{ext}}(u) + \int_{\Omega_a} \left[\lambda^+ \delta u_{,xx} - \lambda^- \delta u_{,xx}\right] \mathrm{d}x. \tag{30}$$

Assuming no body forces, $\delta W_{\mathrm{ext}}(u) = 0$. The first integral can be expanded as

$$\int_{\Omega\setminus\Omega_a} \sigma \delta u_{,x}\,\mathrm{d}x = \int_{\Omega\setminus\Omega_a} (\sigma \delta u)_{,x}\,\mathrm{d}x - \int_{\Omega\setminus\Omega_a} \sigma_{,x} \delta u\,\mathrm{d}x. \tag{31}$$

Observing that $\int_{\Omega\setminus\Omega_a} (\sigma\delta u)_{,x}\,\mathrm{d}x = \int_{\partial(\Omega\setminus\Omega_a)} (\sigma.n)\delta u\,\mathrm{d}x$, where n is the *outward* normal to $\partial(\Omega\setminus\Omega_a)$, the integral becomes

$$\int_{\Omega\setminus\Omega_a} \sigma \delta u_{,x}\,\mathrm{d}x = \int_{\partial(\Omega\setminus\Omega_a)} \left(\sigma^{\Omega\setminus\Omega_a}.n^{\Omega\setminus\Omega_a}\right) \delta u\,\mathrm{d}x - \int_{\Omega\setminus\Omega_a} \sigma_{,x} \delta u\,\mathrm{d}x. \tag{32}$$

Also, $\delta u = 0$ on $\partial\Omega$. Hence,

$$\int_{\Omega\setminus\Omega_a} \sigma \delta u_{,x}\,\mathrm{d}x = \int_{\partial\Omega_a\setminus\partial\Omega} \left(\sigma^{\Omega\setminus\Omega_a}.n^{\Omega\setminus\Omega_a}\right) \delta u\,\mathrm{d}x - \int_{\Omega\setminus\Omega_a} \sigma_{,x} \delta u\,\mathrm{d}x, \tag{33}$$

where $\partial\Omega_a \setminus \partial\Omega$ is the part of the boundary of Ω_a that does not intersect the boundary of Ω (if their intersection is not empty). It shall be observed that in the above equation, $n^{\Omega\setminus\Omega_a}$ is the *outward* normal to $\partial\Omega_a$ part of $\partial(\Omega\setminus\Omega_a)$. The second and the last terms of the equation (30) can be similarly expanded as

$$\begin{aligned}&\int_{\Omega_a} \sigma \delta u_{,x}\,\mathrm{d}x + \int_{\Omega_a} \left[\lambda^+ \delta u_{,xx} - \lambda^- \delta u_{,xx}\right] \mathrm{d}x = \\ &\int_{\partial\Omega_a} \left(\sigma^{\Omega_a}.n^{\Omega_a}\right) \delta u\,\mathrm{d}x - \int_{\Omega_a} \sigma_{,x} \delta u\,\mathrm{d}x + \int_{\Omega_a} \left[\lambda^+ - \lambda^-\right]_{,xx} \delta u\,\mathrm{d}x - \int_{\partial\Omega_a} \left[\lambda^+ - \lambda^-\right]_{,x}.n^{\Omega_a} \delta u\,\mathrm{d}x.\end{aligned} \tag{34}$$

Combining all the above in equation (30),

$$\begin{aligned}\delta^u \Pi^*(u,d,\lambda) = &- \int_{\Omega\setminus\Omega_a} \sigma_{,x} \delta u\,\mathrm{d}x - \int_{\Omega_a} \sigma_{,x} \delta u\,\mathrm{d}x + \int_{\Omega_a} \left[\lambda^+ - \lambda^-\right]_{,xx} \delta u\,\mathrm{d}x + \\ &\int_{\partial\Omega_a} \left(\sigma^{\Omega\setminus\Omega_a}.n^{\Omega\setminus\Omega_a}\right) \delta u\,\mathrm{d}x + \int_{\partial\Omega_a} \left(\sigma^{\Omega_a}.n^{\Omega_a}\right) \delta u\,\mathrm{d}x - \int_{\partial\Omega_a} \left[\lambda^+ - \lambda^-\right]_{,x}.n^{\Omega_a} \delta u\,\mathrm{d}x.\end{aligned} \tag{35}$$

It has been assumed that λ^+ and λ^- are 0 on $\partial\Omega_a$. The equations of equilibrium can be established using $\delta^u \Pi^* = 0$, for arbitrary δu, as (realizing that $n^{\Omega_a} = -n^{\Omega\setminus\Omega_a}$)

$$\sigma_{,x} = 0 \text{ in } \Omega\setminus\Omega_a, \tag{36}$$

$$\sigma_{,x} - [\lambda^+ - \lambda^-]_{,xx} = 0 \text{ in } \Omega_a, \tag{37}$$

$$\sigma^{\Omega\setminus\Omega_a} - \left(\sigma^{\Omega_a} - \left[\lambda^+ - \lambda^-\right]_{,x}\right) = 0 \text{ on } \partial\Omega_a. \tag{38}$$

It shall be noted that the equation (37) resembles the equilibrium equation with the couple stress that arises in the *SG* models [5, 7]. Identifying $\sigma - [\lambda^+ - \lambda^-]_{,x}$ as τ, it can simply be written as $\tau_{,x} = 0$. However, it shall be noted that the term analogous to the *couple stress* is non-zero only in the regions where the constraint is active. In the regions where this is not the case, the equations

of equilibrium remain the same as that in the Cauchy media ($\lambda^{+,-} = 0$ and so, $\sigma = \tau$). This can be regarded as the main difference with the *SG* model, where the couple stresses are active everywhere in the body. The equation (38) resembles the continuity of traction across the internal surfaces, $\sigma = \tau$ at the interface $\partial\Omega_a$.

Remark. Instead of imposing the constraint on the gradient of the strain as in equation (20), it is possible to restrict the strains to be Lipschitz continuous as was done with the damage fields in [15]. However, in the limit of vanishing element length, the constraint on the Lipschitz continuity tends to the constraint on the directional derivative of the strain. It shall be noted that in this case, the regularity requirements on u can be loosened and it is sufficient that $u \in H^1(\Omega)$ as opposed to the currently stated $H^2(\Omega)$. See the Remark 1.

4. FE discretization and solver

4.1. *Discretization*

The minimization problem is solved using the Finite Element method. The choices of the spaces of functions used will be discussed here. As can be observed from the strong form of the equilibrium equations (36) and (37), the Lagrange multipliers take after the *couple stresses* that are usually observed in the *SG* models. Different discretization approaches exist when using the *SG* models [6, 22] - the first, where the displacements are approximated by using Hermite polynomials, the second, considered a mixed FE method, where the displacements are quadratic and an additional strain variable that is piece wise linear linear and continuous. In the second case, the strain variable is constrained to be the gradient of displacement using Lagrange multipliers.

In the present case, the former method will be used and the displacements are approximated in space using Hermite polynomials. Since the Lagrange multipliers are analogous to the couple stresses in the *SG* model, and the couple stresses vary linearly within each element and are discontinuous across elements, a similar discretization will be used for the Lagrange multipliers in this case. Of course, whether the choice of such a space for the Lagrange multipliers is stable should be determined by testing if it satisfies the *inf-sup* condition [23] that typically arises in the class of mixed FE methods. Such a study will be undertaken at a later time and is beyond the scope of the current article. Here, the stability of the solution will be determined by refining the mesh and observing their variations, if any, as the mesh is refined.

The displacement within an element can be expressed as

$$u = u_1 H_1 + u_1' H_2 + u_2 H_4 + u_2' H_3, \tag{39}$$

where

$$H_1(\xi) = 1 - 3\xi^2 + 2\xi^3, \tag{40}$$

$$H_2(\xi) = L\left(\xi - 2\xi^2 + \xi^3\right), \tag{41}$$

$$H_3(\xi) = L\left(-\xi^2 + \xi^3\right), \tag{42}$$

$$H_4(\xi) = 3\xi^2 - 2\xi^3. \tag{43}$$

ξ varies from 0 to 1 with in the element. It can be expressed as a function of the coordinate along the length, x, as $\xi = (x - x_l)/(x_r - x_1)$, where x_1 and x_r denote the coordinates of the left and right nodes, respectively. $L = x_r - x_l$. The representation of the above *shape functions* can be seen in the Figure 1.

The overall displacement field can be written as $u = \boldsymbol{H}\boldsymbol{u}$, where $\boldsymbol{u}$ is a vector containing the degrees of freedom and $\boldsymbol{H}$ is the matrix containing the basis or the shape functions. The strains can be expressed similarly as $\epsilon = \boldsymbol{B}\boldsymbol{u}$, where $\boldsymbol{B}$ is the discrete gradient operator.

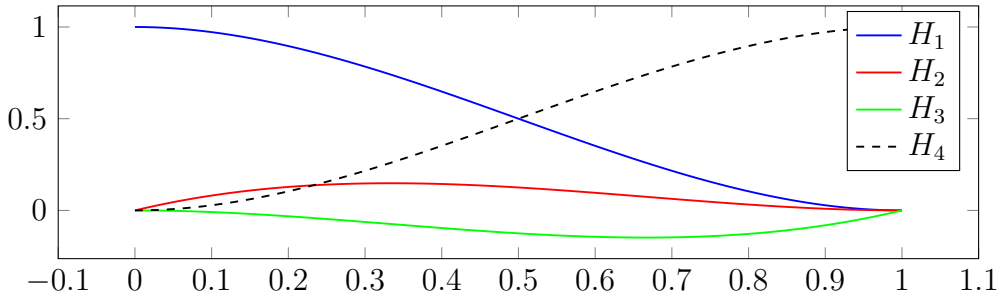

Figure 1. The Hermite polynomial shape functions for an element of unit length.

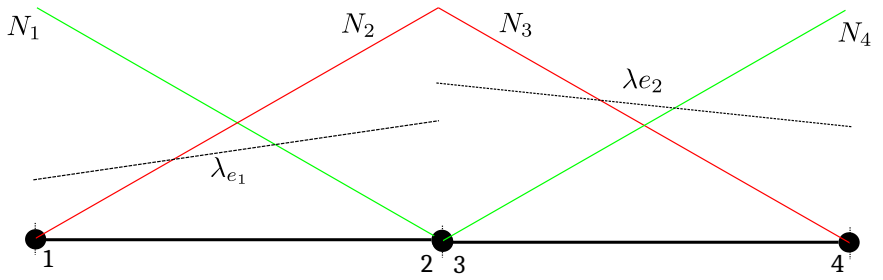

Figure 2. Shape functions for the Lagrange multiplier.

The strain energy density at a point is given by $\psi = \frac{1}{2}E\epsilon^2$. The overall strain energy is hence $\int \psi \, \mathrm{d}x$. This can be expressed as

$$\int_\Omega \psi \, \mathrm{d}x = \sum_{e=1}^{N_e} \int_{\Omega_e} \psi \, \mathrm{d}x, \tag{44}$$

where N_e denotes the number of elements. Within each element, the integral can be computed using an appropriate quadrature rule. For instance, since the displacements are cubic, the strains within each element are quadratic. Strain energy is hence a fourth order polynomial for a homogeneous material. Hence, the Gauss quadrature rule with three integration points can integrate the strain energy density functional exactly. In cases where either the material or the geometry is not homogeneous, the integration is only approximate.

$$\int_{\Omega_e} \psi \, \mathrm{d}x \approx \sum_{g=1}^{3} \frac{1}{2} w_g E_g A_g \epsilon_g^2. \tag{45}$$

In the above, w_g denotes the quadrature weight, E_g and ϵ_g denote the value of modulus and the strain at the integration point, respectively. A_g is the cross-sectional area at the Gauss point. Similar procedure can be followed for all the elements and the overall strain energy can be expressed as

$$\int \psi \, \mathrm{d}x \approx \frac{1}{2} \boldsymbol{u}^T \boldsymbol{K} \boldsymbol{u}. \tag{46}$$

$\boldsymbol{K}$ is the *stiffness* matrix. The damage variable is computed at the Gauss point using the strain variable. In this case, E_g is the *damaged* modulus at the Gauss point, $E_g = g(d_g)E_0$. The minimization is performed using the alternate minimization technique and hence, d_g is a known (see the next section).

As mentioned earlier, the Lagrange multipliers are taken to be piecewise linear and discontinuous, see Figure 2. They can be expressed as $\lambda = \boldsymbol{N}^\lambda \boldsymbol{\lambda}$. $\boldsymbol{\lambda}$ is a vector containing the nodal values

of the Lagrange multiplier. The gradient of the strain can be expressed as $\epsilon' = \boldsymbol{D}\boldsymbol{u}$, where $\boldsymbol{D}$ is the discrete second gradient operator. The inequality constraint, $\epsilon' \leq 1/\ell_c$, written in weak form, becomes

$$\int \lambda \epsilon' \, \mathrm{d}x \leq \int \frac{1}{\ell_c} \lambda \, \mathrm{d}x. \tag{47}$$

Written in terms of the global degrees of freedom,

$$\boldsymbol{\lambda}^T \left(\int \left(\boldsymbol{N}^\lambda \right)^T \boldsymbol{D} \, \mathrm{d}x \right) \boldsymbol{u} \leq \boldsymbol{\lambda}^T \int \frac{1}{\ell_c} (\boldsymbol{N}^\lambda)^T \, \mathrm{d}x. \tag{48}$$

The above equation is integrated numerically by a two point Gauss quadrature rule. The discrete form of the constraint is

$$\Lambda \boldsymbol{u} \leq \boldsymbol{l}_c, \tag{49}$$

where, $\Lambda = \int (\boldsymbol{N}^\lambda)^T \boldsymbol{D} \, \mathrm{d}x$. The constraint $\epsilon' \geq -1/\ell_c$ can be written as $-\epsilon' \leq 1/\ell_c$. In discrete form,

$$-\Lambda \boldsymbol{u} \leq \boldsymbol{l}_c. \tag{50}$$

The two constraint can be written together as

$$\boldsymbol{A}u \leq \boldsymbol{b}, \tag{51}$$

where

$$\boldsymbol{A} = \begin{pmatrix} \Lambda \\ -\Lambda \end{pmatrix} \quad \text{and} \quad \boldsymbol{b} = \begin{pmatrix} \boldsymbol{l}_c \\ \boldsymbol{l}_c \end{pmatrix}.$$

Remark 1. In the current case, since the constraint is imposed on the gradient of strain and this requires the computation of the strain gradient, the Hermite elements have been used. For a linear element, the strain field is constant over an element and the gradient of strain will be 0 within the element. If, instead, as mentioned earlier, the strains are constrained to be Lipschitz continuous, a linear element would have been sufficient.

4.2. *Solver*

The strain energy functional is not convex anymore when the damage variable is introduced. Hence, the alternate minimization algorithm will be used to find the minimum of the strain energy functional. During this process, at a given time step, the minimization is carried out with respect to the displacement variable assuming the damage variable to be frozen. After the displacements are updated, the potential energy is now treated as a function of the damage alone and is minimized with respect to damage. This leads to the update of damage variable according to the equation (8). Convergence is said to have been achieved if, at a given iteration, the change in the displacement and the damage variables are within some tolerance level.

The first minimization with respect to displacement is to be carried out under the inequality constraint in the equation (51). The `fmincon` subroutine of Matlab, with the `SQP` method [24] has been used to carryout this minimization. The subroutine requires the gradient of the objective function to be supplied. In the current case, this is simply $\boldsymbol{K}\boldsymbol{u}$, owing to the quadratic objective function. The discrete form of the inequality constraints is already of the form $\boldsymbol{A}\boldsymbol{u} \leq \boldsymbol{b}$ and need not be simplified any further. The dirichlet boundary conditions on the displacement are applied as equality constraints.

The minimization with respect to the damage variable, together with the form of the function g results in the expression for damage as in equation (14). The damage is updated subject to the constraint $\dot{d} \geq 0$. Written discretely, this translates to $d \geq d_{n-1}$, where d_{n-1} is the damage at the previous time step. In short, if $\widetilde{d} = \frac{\epsilon - \epsilon_0}{\epsilon_f - \epsilon_0}$, $\widetilde{d} = 1$ if $\epsilon \geq \epsilon_f$. $d|_{t=0} = 0$. Then

$$d = \begin{cases} d_{n-1}, & \text{if } \widetilde{d} \leq d_{n-1} \\ \widetilde{d}, & \text{otherwise.} \end{cases} \tag{52}$$

It shall be noted that this update is carried out at each Gauss point.

5. Application to a 1D problem

To test the effectiveness of the formulation in preventing the strain localization, it has been applied to the case of a 1D bar under traction with a *defect* at the center to trigger the initiation and localization of damage. The geometry considered can be seen in Figure 3.

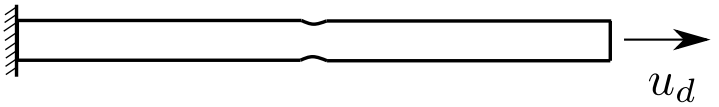

Figure 3. 1D bar used for the analysis. The area at the middle of the bar is slightly smaller than the rest of the bar, which initially allows the strains to localize in that region.

At the center of the bar, the area is taken to vary as $A(x) = 1 + 0.01\cos(\pi - (\pi x)/(2\xi) + \pi/(4\xi))$, $\xi = 0.12\,\text{m}$. The bar is fixed at its left end and is subjected to a displacement at its right end. Characteristic length ℓ_c is chosen so that $1/\ell_c = (\epsilon_f - \epsilon_0)/\ell_{c0}$, that the material that undergoes damage occupies a length of ℓ_{c0} at failure. For the damage model chosen, the parameter ℓ_{c0} can also be related to the energy dissipated by the structure as will be shown later in equation (55).

Remark. The value of $1/\ell_c$ should be chosen to prevent the inequality constraint on the strain gradient from becoming an equality constraint before the initiation of damage.

The value of l_{c0} has been chosen to be 0.2 m. ϵ_0 and ϵ_f have been chosen to be 1×10^{-3} and 15×10^{-3}, respectively. E_0 has been chosen to be 1×10^5 Pa. It is expected that the localization of strain and damage occur at the middle of the bar when u_d approaches 1 mm. The response of the bar will be studied under two different mesh sizes. The region of interest is meshed with elements of smaller length compared to the edges. It was ensured that the potential localization region is resolved by at least 10 elements.

Remark. It will be observed later on that the value of ℓ_{c0} chosen leads to a snap-back in the overall traction-separation behavior of the body. To capture this response, an arc-length based solver that controls the amount of dissipation in a time step [25] has been used.

5.1. *Results*

The distribution of strain (before the initiation of damage) along the bar when the bar is meshed with 35 elements can be seen in the Figure 4. Here, the strain gradient remains strictly below $1/\ell_c$ and so, the constraint is inactive. It shall be noted that the element size is nonuniform - the body is divided into three regions. In the regions away from the center, the element size has been chosen to be 0.06 m. Near the center where the damage is expected to occur, the element size is about 0.016 m.

As a consequence of the smaller cross-sectional area at the center of the bar, the strains are higher in that region. As the value of u_d increases, the damage, hence, initiates at the center and propagates outward. The evolution of damage as the displacement at different times can be seen in the Figure 5 for when the bar is meshed with 35 and 55 elements. It shall be noted that the regions away from the center (where the element size is 0.06 m) are not refined. Only the central part of the bar of about 0.4 m has been refined between the two mesh sizes. The applied displacement values for each curve starting from the lower most to the upper most curves

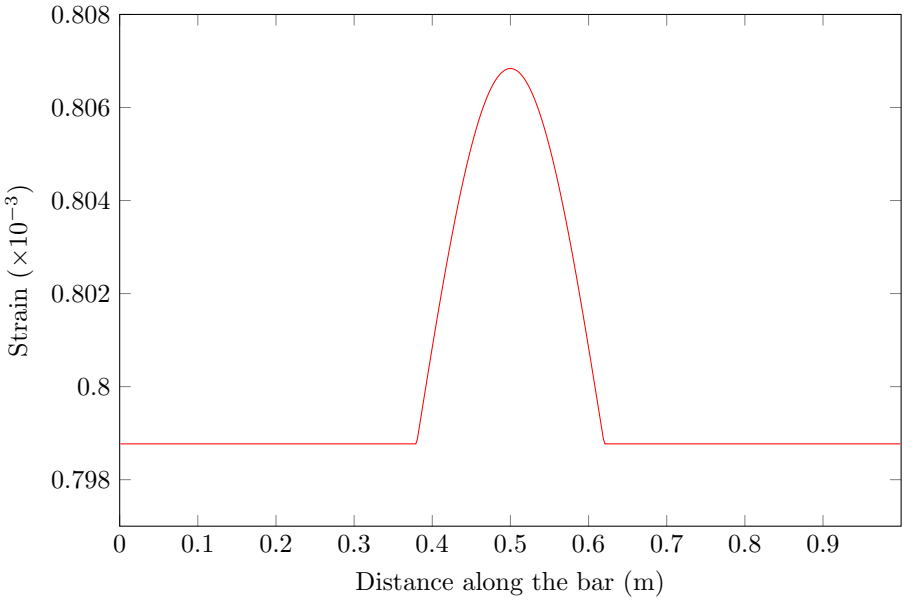

Figure 4. Strain distribution along the bar when applied displacement = 0.8017 m. The constraint is not yet active at this time.

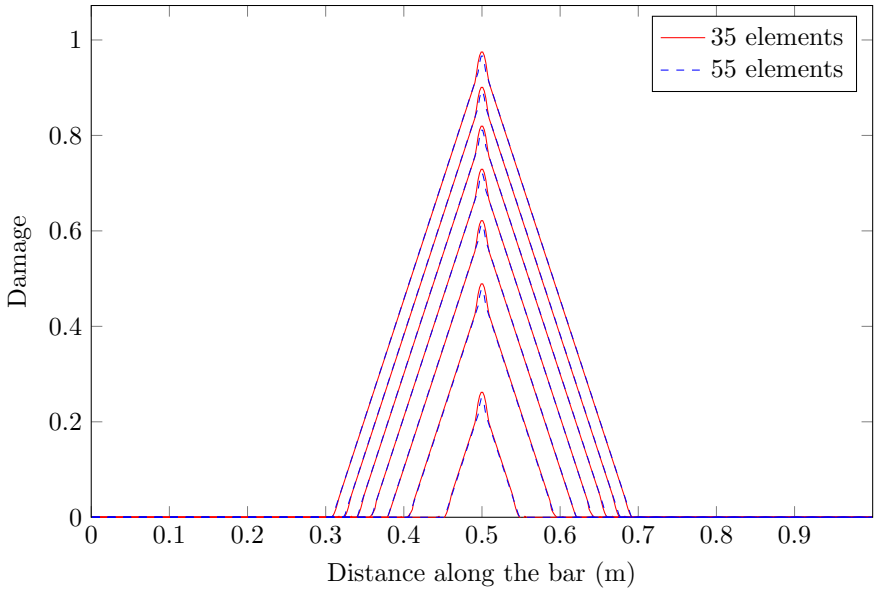

Figure 5. Distribution of damage along the bar meshed with 35 and 55 elements. The applied displacement values for each curve starting from the lower most to the upper most curves are 1.0492 mm, 1.4206 mm, 1.7919 mm, 2.1633 mm, 2.5346 mm, 2.9060 mm, and 3.2773 mm.

are 1.0492 mm, 1.4206 mm, 1.7919 mm, 2.1633 mm, 2.5346 mm, 2.9060 mm, and 3.2773 mm. The corresponding distribution of strain can be seen in the Figure 6 for the two meshes. Also can be seen in dashed line is the case where the bar is completely broken and the strain is concentrated in the element that is fully damaged ($d = 1$).

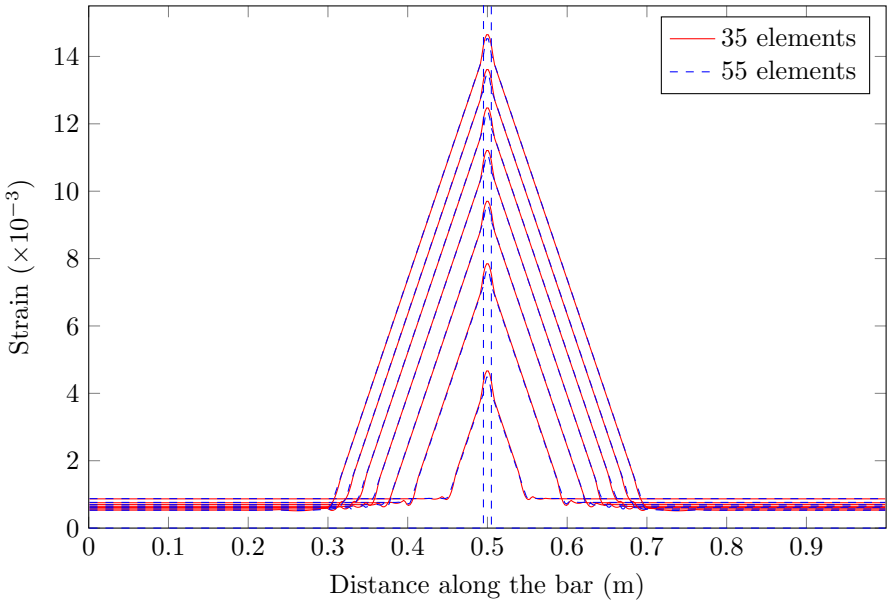

Figure 6. Distribution of strain along the bar meshed with 35 and 55 elements. The applied displacement values for each curve starting from the lower most to the upper most curves are 1.0492 mm, 1.4206 mm, 1.7919 mm, 2.1633 mm, 2.5346 mm, 2.9060 mm, and 3.2773 mm.

From both the results, it can be seen that the length of the damaged region remains the same at the instant when the center of the bar is fully damaged even when the mesh is refined. This span can be seen to be $2\ell_{c0}$. The overall response of the bar presented as the load vs displacement plot can be seen in the Figure 7. The results for the two mesh sizes can be seen to be almost similar.

To compare the effect of the parameter ℓ_{c0} on the width of the damaged region, its value has been changed to 0.1 m and the computations presented above have been repeated. The damage profile when the bar is completely broken along with the case where $\ell_{c0} = 0.2$ m can be seen in the Figure 8. The load-displacement curve when $\ell_{c0} = 0.1$ m can be seen in the Figure 9.

The paths taken by different point in the body can be seen on the stress-strain plot in the Figure 10. It can be seen that the point at the center takes up all the strain once it is fully damaged. The rest of the points in the damage zone then undergo unloading to the origin. The point that is away from the damage zone simply undergoes loading and unloading on the elastic branch.

5.2. *Variation of the Lagrange multipliers*

In the region where the constraint on the strain gradient is active, it is expected that the Lagrange multipliers are non-zero. It shall be noted that the Lagrange multipliers are analogous to the couple stresses that arise in the strain gradient theory. The distribution of Lagrange multipliers along the bar at an instance when the bar is partially damaged can be seen in Figure 11. The variation of the Cauchy stress, σ, along the bar at the same time step can be seen in the Figure 12. The evolution of Lagrange multipliers when the bar is meshed by 55 elements for the same load cases for the strains presented earlier can be seen in the Figure 13. It can be seen that the region where the Lagrange multipliers are non zero expand further into the body with the damage front. It can be seen that σ is not homogeneous in the regions where the Lagrange multipliers are non-zero.

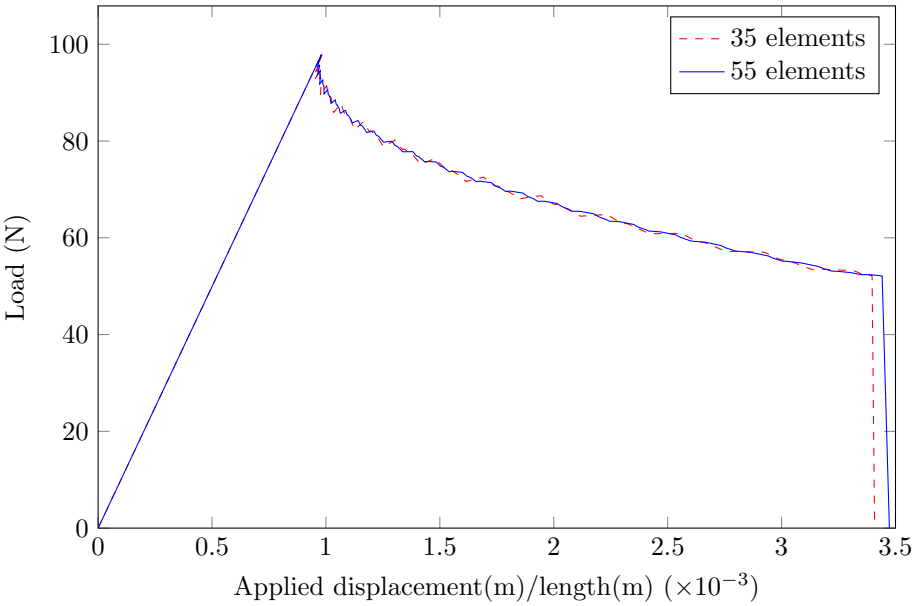

Figure 7. Overall load-displacement response of the bar with two different meshes (ℓ_{c0} = 0.2m).

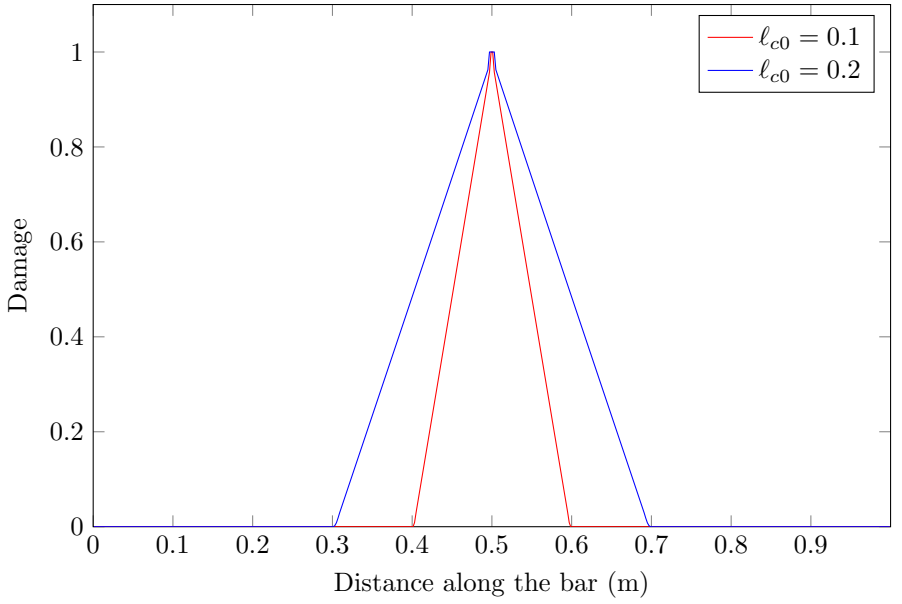

Figure 8. Damage profile when the bar breaks for ℓ_{c0} = 0.1 m and 0.2 m.

It can be noticed from the Figures 6 and 12 that the strains as well as the stresses exhibit oscillations towards the end of localization zone. These can be attributed to the sharp rise in the strains as the localization zone expands. This, in combination with the order of interpolation used may result in oscillations in the strains and stresses. If linear elements were used together with the Lipschitz constraint, the oscillations might not have occurred.

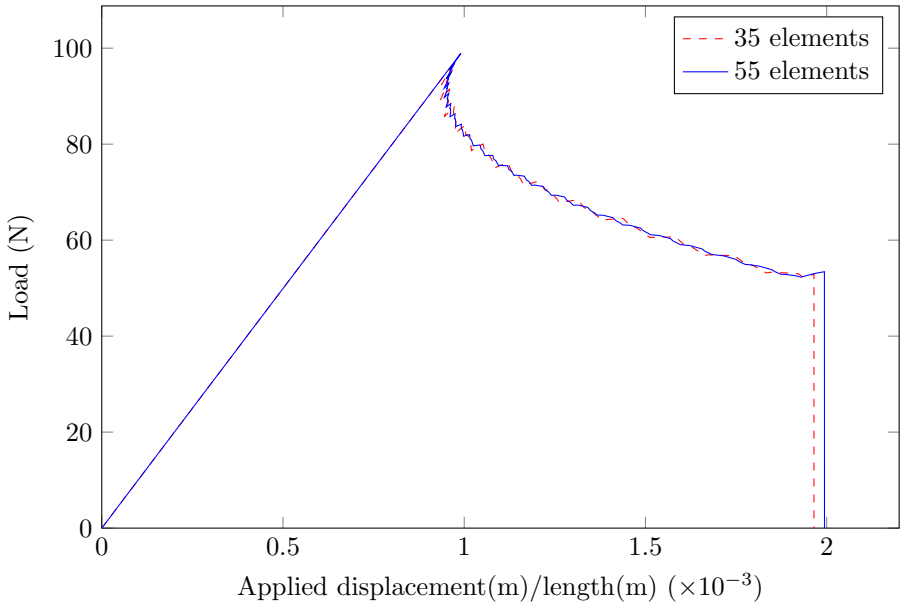

Figure 9. Overall load-displacement response of the bar with two different meshes (ℓ_{c0} = 0.1 m).

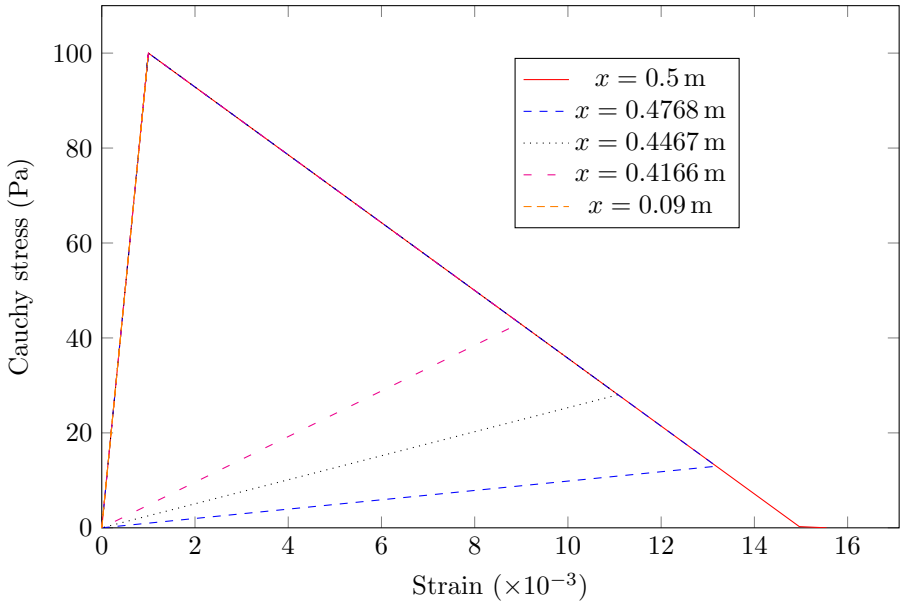

Figure 10. The paths taken by different points in the body with their positions as in the legend. Here, $\ell_{c0} = 0.2$ m.

5.3. *Verification of equilibrium*

The strong form of the equilibrium equations obtained by using the current regularization method can be seen in the equations (36) and (37). The weak form of these equations can be seen in the equation (29). Whether the Cauchy stress and Lagrange multipliers obtained from the current simulations satisfy the equilibrium equations can be verified by using them in the

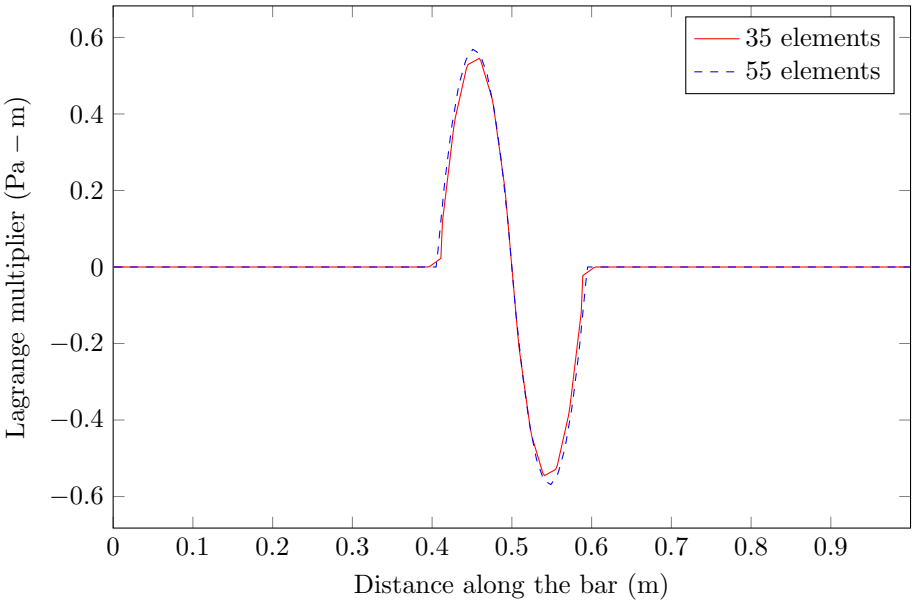

Figure 11. Variation of Lagrange multiplier ($\lambda^+ - \lambda^-$) along the bar, for an applied displacement of 1.4206 mm.

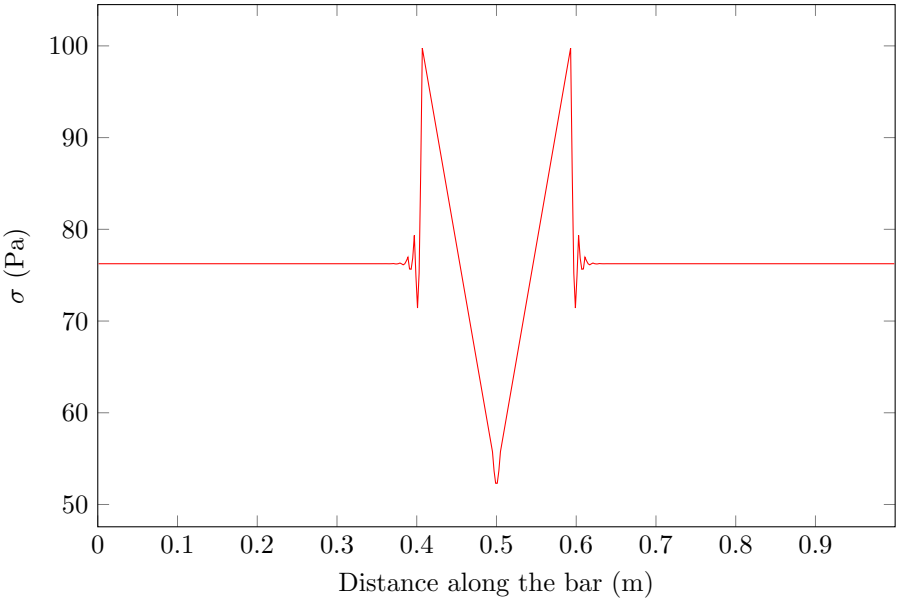

Figure 12. Variation of σ along the bar, meshed with 55 elements, for an applied displacement of 1.4206 mm.

equation (29). Observing that the virtual work of the internal forces can be written in the form (see equation (29) for definitions) $\delta W_\sigma + \delta W_\lambda = \{\delta \boldsymbol{u}\}^T \{\boldsymbol{f}\}_{int}$, at equilibrium, it is expected that $\{\boldsymbol{f}\}_{int} = \mathbf{0}$ for the internal nodes. For the nodes at the boundary, non-zero values corresponding to the reaction forces are expected.

Defining $\delta W_\sigma = \{\delta \boldsymbol{u}\}^T \{\boldsymbol{f}\}_\sigma$ and $\delta W_\lambda = \{\delta \boldsymbol{u}\}^T \{\boldsymbol{f}\}_\lambda$ (see equation (29)), the variation of $\{\boldsymbol{f}\}_\sigma$ and $\{\boldsymbol{f}\}_\lambda$ as a function of the number of the degree of freedom can be seen in Figure 14.

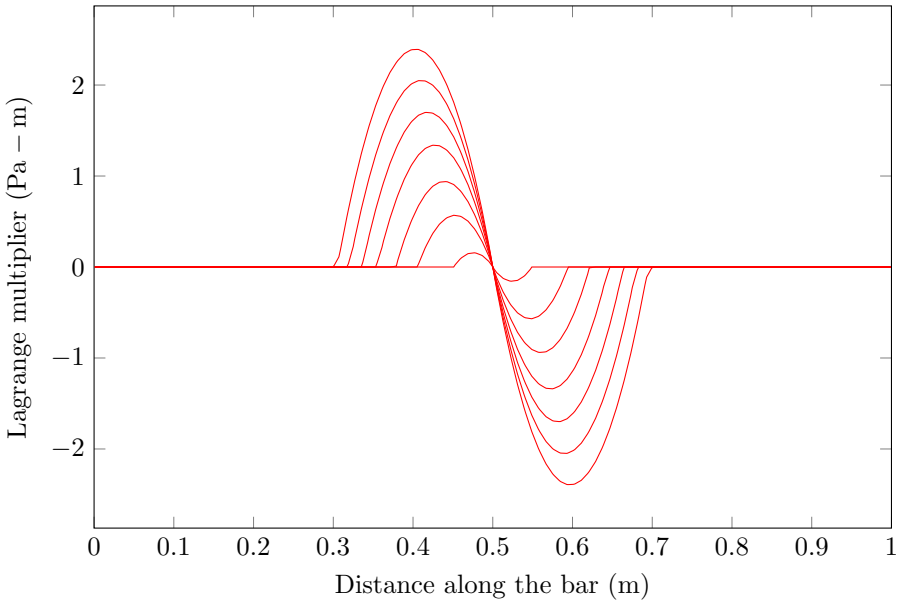

Figure 13. Variation of Lagrange multiplier ($\lambda^+ - \lambda^-$) along the bar, for various end displacements. The applied displacement values for each curve starting from the lower most to the upper most curves are 1.0492 mm, 1.4206 mm, 1.7919 mm, 2.1633 mm, 2.5346 mm, 2.9060 mm, and 3.2773 mm.

Non zero values of the internal forces, $\boldsymbol{f}_\sigma$, can be seen at the internal nodes in contrast to what is usually seen in the unconstrained case. The force $\boldsymbol{f}_\lambda$ can be seen to take equal values but with opposite signs. The evolution of the internal force vector, $\{\boldsymbol{f}\}_{int} = \{\boldsymbol{f}\}_\sigma + \{\boldsymbol{f}\}_\lambda$, can be seen in the Figure 15. Here, the only non-zero forces observed are at the ends of the bar, corresponding to the displacement degrees of freedom, as expected. Hence, it can be concluded that the Cauchy stress and the Lagrange multipliers together verify the weak form of the equilibrium equation.

Remark. It shall be noted that since the Hermite elements have been used in this article, the degrees of freedom at a node is the displacement and its derivative. The global degrees of freedom are stored in an array of the form $\{u_1\ u_1'\ u_2\ u_2'\ \ldots\}^T$. The conjugate nodal forces take the form $\{f_1\ m_1\ f_2\ m_2\ \ldots\}^T$. At the boundaries of the body, only the displacements are applied, and hence, only the nodal forces that are conjugate to the displacement appear. Hence, in the Figure 15, at the right end, the penultimate force can be observed to be non-zero, while the last DOF that is conjugate to the derivative of displacement can be seen to be zero.

5.4. *Significance of regularization region*

It shall be noted that the constraints on the gradient of strains are active only in the region of the body where the damage is smaller than 1. The reason for this will be discussed here. It has been noted earlier on in the article that the Lagrange multipliers that enforce the constraint on the gradient of the strain are analogous to the couple stresses that are encountered in the strain gradient models.

The regularization used in the current study can be interpreted as that in the *SG* models, but with some differences. In the *SG* models, the modulus (E') associated with the strain gradient affects the solution in the regions where the strain gradient is non-zero. This is the case regardless

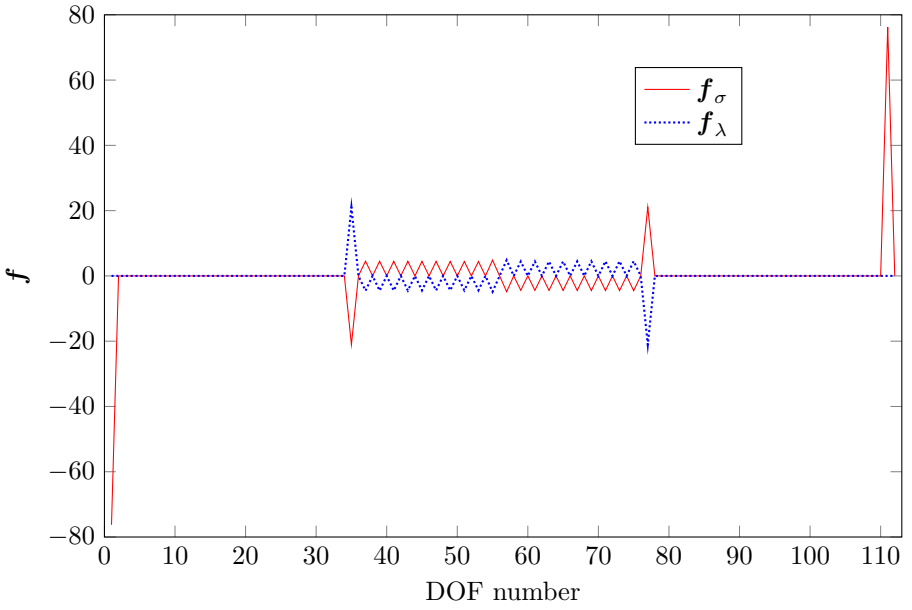

Figure 14. Internal nodal forces, $\{\boldsymbol{f}\}_\sigma$ and $\{\boldsymbol{f}\}_\lambda$, as a function of the number of degree of freedom, for an applied displacement of 1.4206 mm.

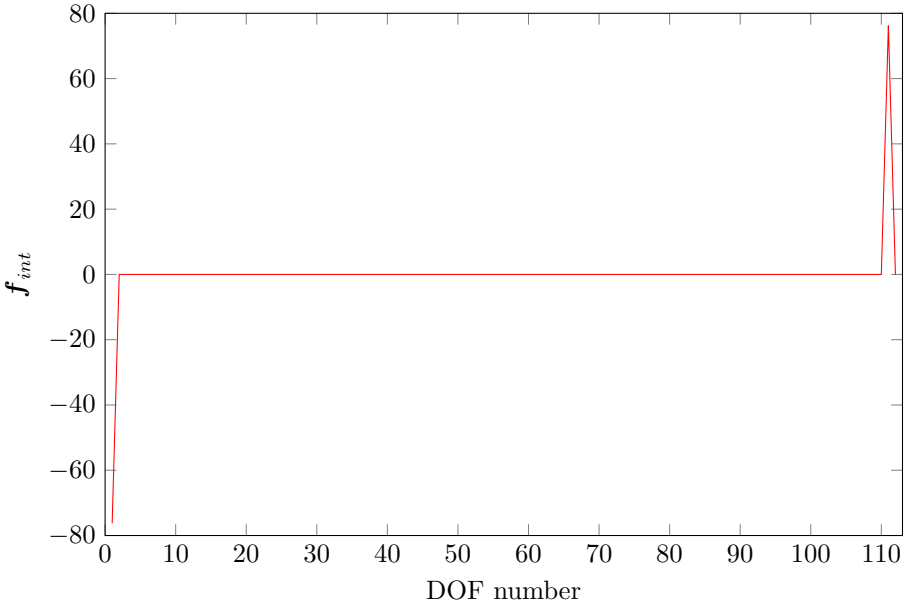

Figure 15. Internal nodal forces, $\{\boldsymbol{f}\}_{int} = \{\boldsymbol{f}\}_\sigma + \{\boldsymbol{f}\}_\lambda$, as a function of the number of degree of freedom, for an applied displacement of 1.4206 mm.

of whether the material is undergoing damage or not. In the current case, however, it shall be noted that for the regularization to be active, the gradient of strain should be equal to $1/\ell_{c0}$. When the strain gradients are smaller than this value, the constraint is inactive and the solution coincides with the elastic solution (gradient independent elasticity). When the damage initiates, the element in which the initiation takes place deforms more than the rest, which increases the

gradient of strain as the surrounding elements are possibly undamaged. The constraint is thus activated after the damage and hence the strain increases to a certain level, which results in the propagation of strain and hence damage to the surrounding elements. The non-locality is thus achieved.

Deactivating the constraint once again when the damage reaches 1 lets the damaged element take up all the deformation (currently, regularization is removed from an element if the damage at any of the Gauss points reaches 0.999). This also prevents the damage envelope from expanding into the body as the strains are increased, limiting the damage to a band of width ℓ_{c0}, regardless of the length of the bar. Hence, the energy dissipated during the process does not depend on the length of the bar. This can be noted to be one of the main differences between the current regularization technique and the strain gradient models.

An analysis of the *SG* models in the context of regularizing the damage problem can be seen in [7]. Two cases were considered in that article. In the first case, the damage variable is taken to act only on the modulus (E) associated with the strain and not on the modulus (E') associated with the strain gradient. In this case, it was observed that the energy dissipated in the bar (from the initiation of damage till the stresses in the bar become zero) depends on the length of the bar and that for a bar of infinite length, this is ∞. It was concluded that this was the case even when the damage acts on E', but $E'(1)$, the modulus when the material is fully damaged, is strictly greater than 0.

It was also observed in the same study that making E' a function of the damage variable such that E' goes to 0 when the damage reaches 1 results in an ineffective regularization. In essence, the results of the FE simulations were observed to depend on the mesh size in this case. In the simulations performed in that study, the dependence of E' on the damage variable was taken to be similar to that of E. Such effects are avoided in the present approach.

5.5. *Energy balance*

The energy dissipated in the body as it undergoes damage can be seen to be $D|_0^t = \int_\Omega Y_c d(t)\,\mathrm{d}x$. Since the final damage profile can be observed to not depend on the mesh size (see Figure 5), the energy dissipated in the body is hence independent of the mesh size. The energy dissipated in the body from the damage initiation to complete fracture can be related to the parameter ℓ_{c0} as follows. When the damage reaches 1 (and hence, ϵ reaches ϵ_f) at some point in the body, the strain distribution in the damaged region can be written as (as a consequence of the Lipschitz constraint)

$$\epsilon(x) = \epsilon_0 + \frac{\epsilon_f - \epsilon_0}{\ell_{c0}} x, \quad \forall\, x \in [0, \ell_{c0}], \tag{53}$$

where the x-coordinate is taken as 0 at the point where $\epsilon = \epsilon_0$. The damage variation in this region, from equation (14), can be seen to be

$$d(x) = \frac{x}{\ell_{c0}}. \tag{54}$$

The energy dissipated in the body is $\int_\Omega Y_c d\,\mathrm{d}x = 2Y_c \int_0^{\ell_{c0}} d\,\mathrm{d}x$ (since the damaged material spans a length of $2\ell_{c0}$). Since $Y_c = -g'(0)\psi_0(\epsilon_0)$, the expression for the energy dissipated (denoted as G_c) can be seen to be

$$G_c = \int_\Omega Y_c d\,\mathrm{d}x = \frac{k}{2} E_0 \epsilon_0^2 \ell_{c0} \; (= Y_c \ell_{c0}). \tag{55}$$

The parameters k, E_0, ϵ_0, and ℓ_{c0} have been defined earlier. Hence, fixing all other parameters and changing ℓ_{c0} results in a different G_c. Thus, changing ℓ_{c0} while keeping all the other parameters the same is akin to analyzing a material with a different G_c.

The evolution of the strain energy (SE= $\int \psi\,\mathrm{d}x$), energy dissipated (D= $\int_\Omega Y_c d\,\mathrm{d}x$) and the total external work ($\mathrm{W}_{ext} = \int_0^t f_{ext}(t)\dot{u}\,\mathrm{d}t$) done on the body can be seen in the Figure 17 when

$\ell_{c0} = 0.2\,\text{m}$ and in the Figure 18 when $\ell_{c0} = 0.1\,\text{m}$ for two meshes presented earlier. Till the initiation of damage, it can be observed that $W_{ext} = \text{SE}$. The dissipation in the body can be seen to increase as the damage evolves and the damage front moves into the body. It shall be noted that the evolution of energies has been plotted with the ratio of maximum strain in the bar at each time to the strain at failure (ϵ_f) since this quantity is monotonically increasing.

With the parameters chosen, the value of G_c can be computed from equation (55) and compared with the dissipation obtained from the FE computations. For $\ell_{c0} = 0.1\,\text{m}$, and $0.2\,\text{m}$, the values of G_c are $0.15\,\text{J}$ and $0.075\,\text{J}$, respectively. The corresponding values obtained from the FE computations using the finer mesh can be seen to be $0.145\,\text{J}$ and $0.0723\,\text{J}$, respectively and are quite close to the expected values.

From Figure 17, it can be seen that the strain energy in the body increases towards the end as the material undergoes failure in the case of $\ell_{c0} = 0.2\,\text{m}$. However, when $\ell_{c0} = 0.1\,\text{m}$ (Figure 18), there is a reduction in the strain energy as the damage progresses. This can be interpreted as follows. The strain energy in the body can be written as

$$SE = \int_\Omega \psi \,\mathrm{d}x = \int_{\Omega_u} \psi \,\mathrm{d}x + \int_{\Omega_d} \psi \,\mathrm{d}x, \tag{56}$$

where Ω_u denotes the undamaged region of the body ($d(x) = 0 \;\forall\; x \in \Omega_u$) and Ω_d denotes the region of the body undergoing damage ($d(x) > 0 \;\forall\; x \in \Omega_d = \Omega \setminus \Omega_a$). The measure of Ω_d depends on the parameter ℓ_{c0}. Also, the values taken by the strain energy density, ψ, in Ω_d depends on the parameters of the damage evolution model such as k. For instance, the variation of the strain energy density with strain for two different values k can be seen in Figure 16. The strain energy density function has been expressed entirely in terms of the strain variable only, $\psi(u,d) = g(d(\epsilon))\psi_0(\epsilon)$. It can be seen that the variation of ψ after the initiation of damage is a competition between the increasing strain and damage variables. It shall be noted that the ψ that enters the second term on the RHS of equation (56) belongs to the region marked *undergoing damage* in Figure 16. Hence, even though the measure of the region Ω_d might be smaller than the measure of Ω_u, the strain energy density in Ω_d might be higher than in Ω_u which leads to different variations of SE after the initiation of damage depending on the parameters such as k, ℓ_{c0}.

Figure 19 presents the energy evolution for cases where ϵ_f and ℓ_{c0} are varied. For the case where $\epsilon_f = 7.5 \times 10^{-3}$, $\ell_{c0} = 0.2\,\text{m}$ (dashed lines), $G_c = 0.075\,\text{J}$ is same as when $\epsilon_f = 15 \times 10^{-3}$, $\ell_{c0} = 0.1\,\text{m}$. It can be seen that the energy dissipated for both the cases is the same. The value of abscissa when the damage (and hence dissipation) initiates is different because of the different ϵ_fs. Once initiated, the evolution curves for both the cases follow a similar trend.

The results for $\epsilon_f = 7.5 \times 10^{-3}$ and $\ell_{c0} = 0.1\,\text{m}, 0.2\,\text{m}$ can be seen in Figure 20. The strain energy can be seen to decrease as the material undergoes damage when $\ell_{c0} = 0.1\,\text{m}$ as the damaged material occupies a smaller region. Also, the ψ vs ϵ curve looks like the solid red line in Figure 16 and hence the strain energy density in Ω_d is smaller when compared to when $\epsilon_f = 15 \times 10^{-3}$.

6. Extension to 2D and 3D cases

The extension of the local damage problem to 2D and 3D cases is straightforward and has been carried out in several references and will be described below briefly. It is of interest here to determine the quantity on which the constraint is to be applied. In the 1D case presented in this article, the constraint has been directly applied on the gradient of the strain variable as the damage is a function of the strain itself. Introducing the constraint on the spatial distribution of strain variable thus prevents the spurious strain and damage localization.

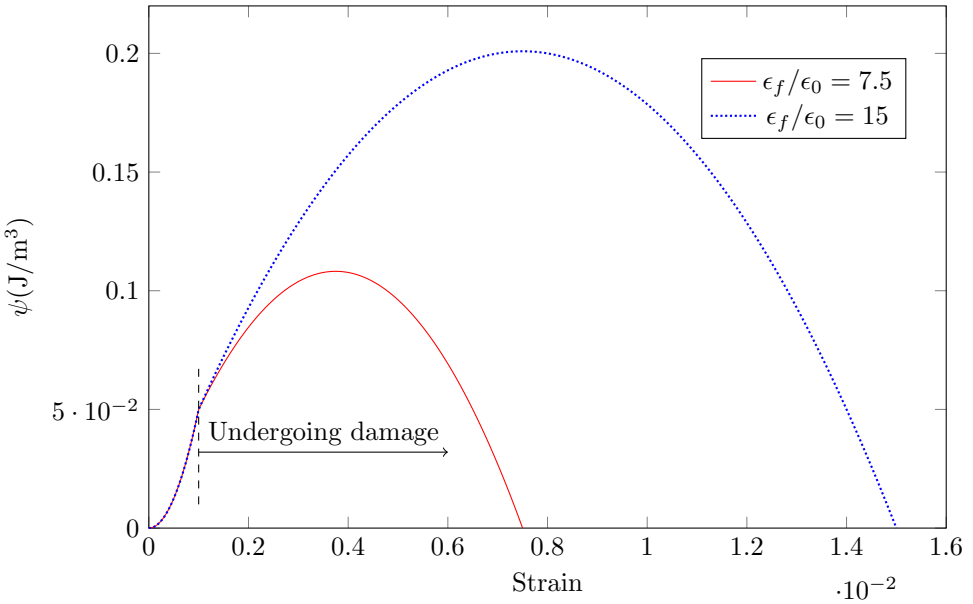

Figure 16. Variation of ψ with strain for different values of $k = \epsilon_f/\epsilon_0$.

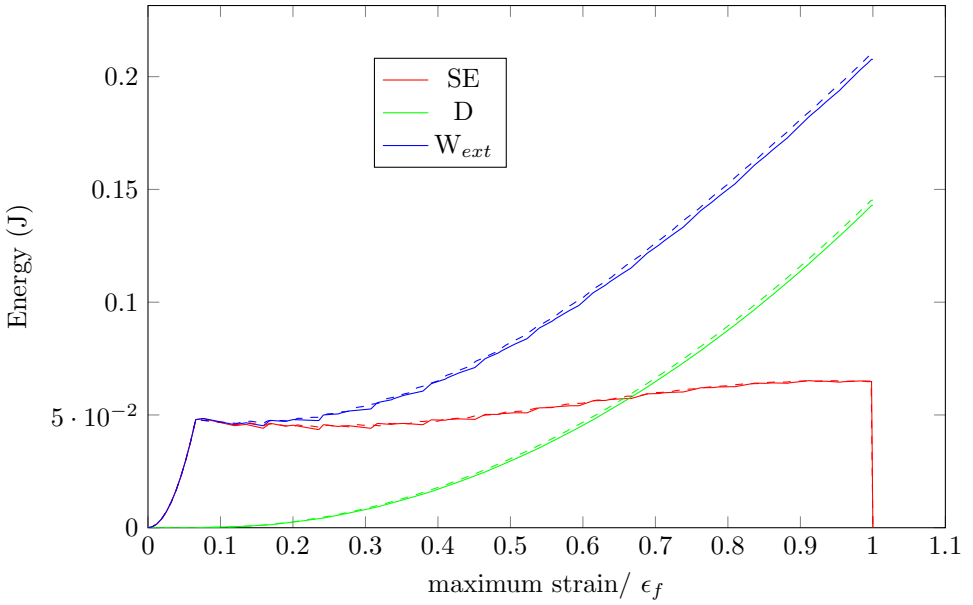

Figure 17. Evolution of different energies plotted as a function of ratio of the maximum strain in the body at each time to ϵ_f. Here, $\ell_{c0} = 0.2\,\mathrm{m}$. The solid and the dashed lines indicate the results when 35 and 55 elements, respectively, are used.

In 2D and 3D cases, the damage is a function of an equivalent strain. The appropriate quantity can be obtained by considering the equation (10), which can be written as

$$Y = -g'(d)\psi_0(\epsilon), \tag{57}$$

where ψ_0 denotes the *undamaged* strain energy functional. Damage propagation is taken to

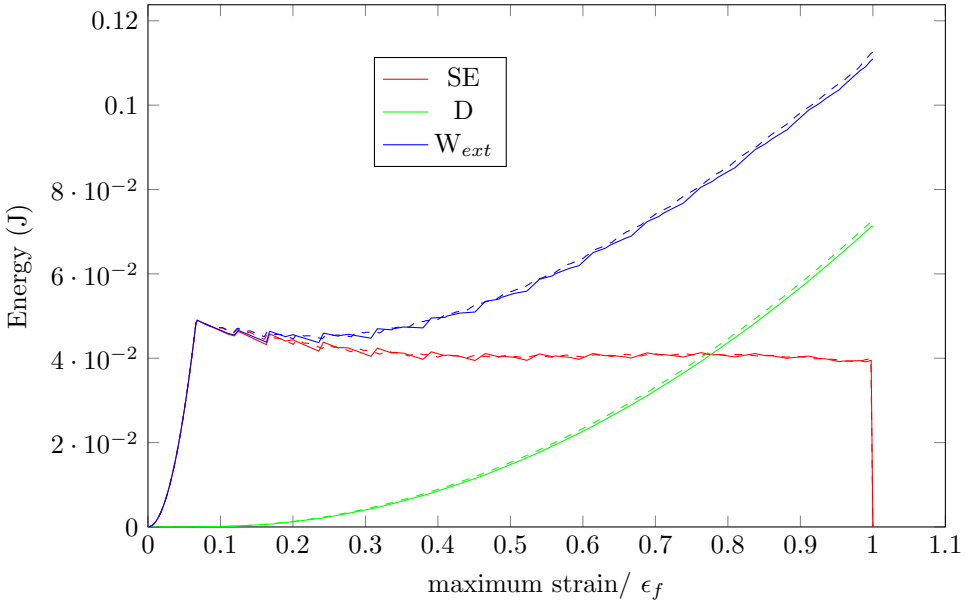

Figure 18. Evolution of different energies plotted as a function of ratio of the maximum strain in the body at each time to ϵ_f. Here, $\ell_{c0} = 0.1\,\text{m}$. The solid and the dashed lines indicate the results when 35 and 55 elements, respectively, are used.

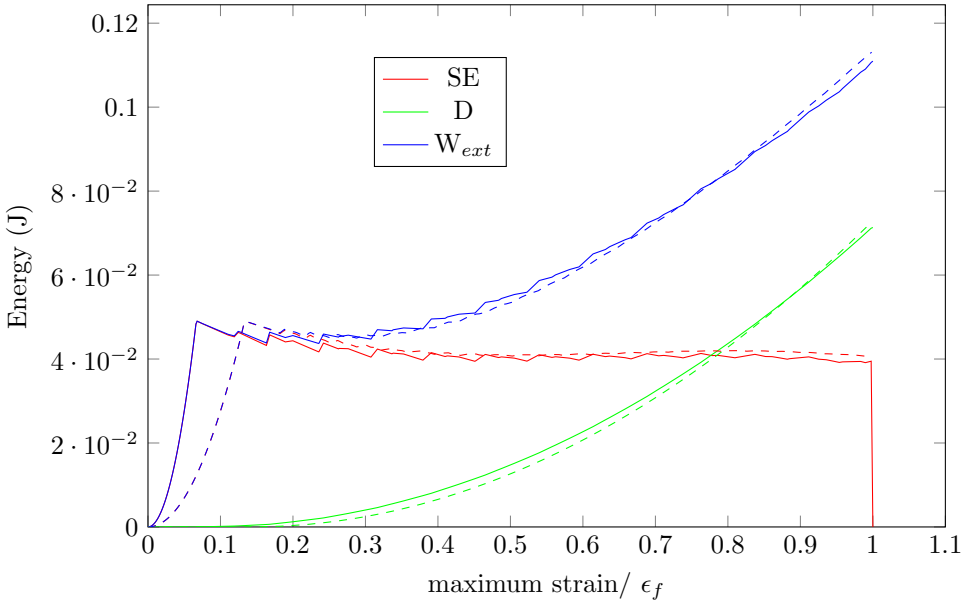

Figure 19. Evolution of different energies plotted as a function of ratio of the maximum strain in the body at each time to ϵ_f.The solid lines are the results when $\epsilon_f = 15 \times 10^{-3}$, and $\ell_{c0} = 0.1\,\text{m}$ while the dashed lines present the results when $\epsilon_f = 7.5 \times 10^{-3}$, and $\ell_{c0} = 0.2\,\text{m}$.

occur when $Y = Y_c$. This condition is then used to determine the damage value at the current time. Equation (12) now becomes

$$d = \left(g'\right)^{-1}\left(\frac{-Y_c}{\psi_0(\epsilon)}\right), \quad \psi_0(\epsilon) \neq 0. \tag{58}$$

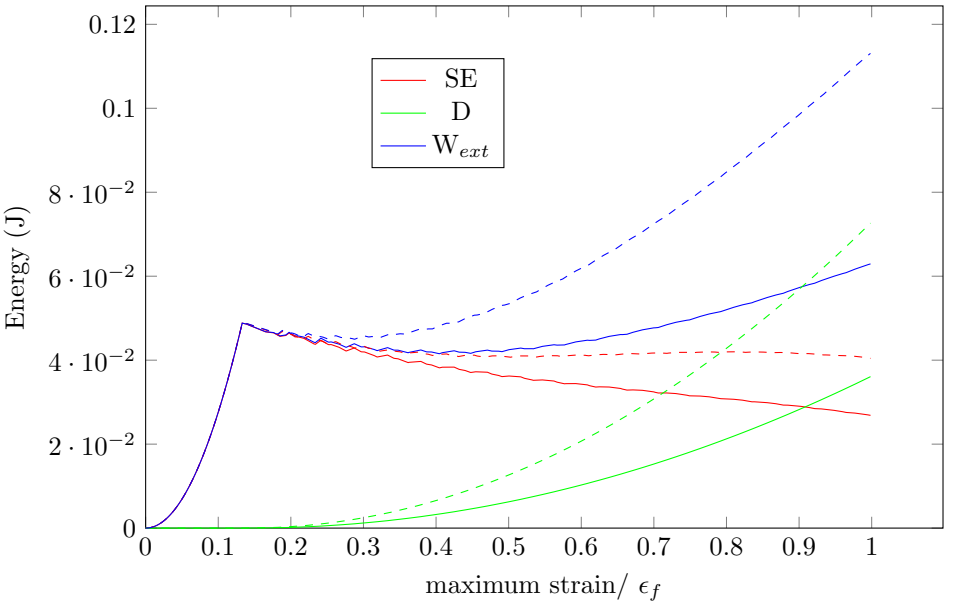

Figure 20. Evolution of different energies plotted as a function of ratio of the maximum strain in the body at each time to ϵ_f.The solid lines are the results when $\epsilon_f = 7.5 \times 10^{-3}$, and $\ell_{c0} = 0.1\,\text{m}$ while the dashed lines present the results when $\epsilon_f = 7.5 \times 10^{-3}$, and $\ell_{c0} = 0.2\,\text{m}$.

By taking the form of g as in the equation (13), an explicit expression for damage can be written as

$$d = \frac{\sqrt{k\psi_0(\epsilon)} - \sqrt{Y_c}}{(k-1)\sqrt{Y_c}}. \tag{59}$$

k can now be seen as $\sqrt{\psi_0(\epsilon_f)/\psi_0(\epsilon_0)}$, the ratio of undamaged strain energies at complete failure to at initiation.

To maintain parallels with the strain gradient elasticity as was done in the case of 1D model, it is possible to impose the constraint directly on the *invariants* of the strain gradients defined through the energy density functional as in [5]. For instance, the constraint can be written as

$$\widetilde{\psi}(\nabla\epsilon) = a_1 k_{iik}k_{kjj} + a_2 k_{ijj}k_{ikk} + a_3 k_{iik}k_{jjk} + a_4 k_{ijk}k_{ijk} + a_5 k_{ijk}k_{kji} \leq \frac{1}{\ell_c'^2}, \tag{60}$$

for some ℓ_c', where $k_{ijk} = \epsilon_{ij,k}$. Taking all the a_i s except a_4 to be 0 results in (for 1D case)

$$\left(u_{,xx}\right)^2 \leq \frac{1}{a_4 \ell_c'^2}. \tag{61}$$

If $a_4\ell_c'^2 = \ell_c^2$, the constraint becomes similar to that of the equation (20).

7. Conclusions

The current article presents a way to introduce a length scale into the problem to prevent the mesh dependence of the solution in case of a softening material. Applying the constraints on the strain instead of damage precludes the need for internal variables. Hence, this approach is ideally suited for applications that use *DDCM*, where the constitutive model used in this article will be replaced by the stress-strain data (i.e. damage variable will not be considered explicitly). It has been observed that the introduction of length scale in such a way renders the solution independent of the finite element mesh even after the initiation of damage. Restricting the

regularization region to where the damage variable is smaller than 1 makes sure that the damage front does not propagate all through the body as is usually observed in the *SG* models (if damage is not directly available, stress can give an indication of the damage level). Thus, the energy dissipated is independent of the geometry of the body and is finite. The extension of the current method to the $2D$ and $3D$ cases will be the subject of future work.

Conflicts of interest

The authors have no conflict of interest to declare.

References

[1] R. H. J. Peerlings, "Enhanced damage modelling for fracture and fatigue", PhD Thesis, Technische Universiteit Eindhoven, Eindhoven, Deutschland, 1999.
[2] R. H. J. Peerlings, M. G. D. Geers, R. De Borst, W. A. M. Brekelmans, "A critical comparison of nonlocal and gradient-enhanced softening continua", *Int. J. Solids Struct.* **38** (2001), no. 44-45, p. 7723-7746.
[3] R. H. J. Peerlings, R. De Borst, W. A. M. Brekelmans, M. G. D. Geers, "Localisation issues in local and nonlocal continuum approaches to fracture", *Eur. J. Mech., A, Solids* **21** (2002), no. 2, p. 175-189.
[4] G. Pijaudier-Cabot, Z. P. Bažant, "Nonlocal damage theory", *J. Eng. Mech.* **113** (1987), no. 10, p. 1512-1533.
[5] R. D. Mindlin, N. N. Eshel, "On first strain-gradient theories in linear elasticity", *Int. J. Solids Struct.* **4** (1968), no. 1, p. 109-124.
[6] Z. C. Xia, J. W. Hutchinson, "Crack tip fields in strain gradient plasticity", *J. Mech. Phys. Solids* **44** (1996), no. 10, p. 1621-1648.
[7] T. Le Duc, J.-J. Marigo, C. Maurini, S. Vidoli, "Strain-gradient vs damage-gradient regularizations of softening damage models", *Comput. Methods Appl. Mech. Eng.* **340** (2018), p. 424-450.
[8] E. Lorentz, S. Andrieux, "Analysis of non-local models through energetic formulations", *Int. J. Solids Struct.* **40** (2003), no. 12, p. 2905-2936.
[9] K. Pham, J.-J. Marigo, C. Maurini, "The issues of the uniqueness and the stability of the homogeneous response in uniaxial tests with gradient damage models", *J. Mech. Phys. Solids* **59** (2011), no. 6, p. 1163-1190.
[10] J.-J. Marigo, C. Maurini, K. Pham, "An overview of the modelling of fracture by gradient damage models An overview of the modelling of fracture by gradient damage models An overview of the modelling of fracture by gradient damage models", *Meccanica* (2016), no. 12, p. 51.
[11] C. Miehe, L. M. Schänzel, "Phase field modeling of fracture in rubbery polymers. Part I: Finite elasticity coupled with brittle failure", *J. Mech. Phys. Solids* **65** (2014), no. 1, p. 93-113.
[12] C. Miehe, L. M. Schänzel, H. Ulmer, "Phase field modeling of fracture in multi-physics problems. Part I. Balance of crack surface and failure criteria for brittle crack propagation in thermo-elastic solids", *Comput. Methods Appl. Mech. Eng.* **294** (2015), p. 449-485.
[13] N. Moës, C. Stolz, P. E. Bernard, N. Chevaugeon, "A level set based model for damage growth: The thick level set approach", *Int. J. Numer. Methods Eng.* **86** (2011), no. 3, p. 358-380.
[14] N. Valoroso, C. Stolz, "Graded damage in quasi-brittle solids", *Int. J. Numer. Methods Eng.* **123** (2022), no. 11, p. 2467-2498.
[15] N. Moës, N. Chevaugeon, "Lipschitz regularization for softening material models: The Lip-field approach", *Comptes Rendus. Mécanique* **349** (2021), no. 2, p. 415-434.
[16] T. Kirchdoerfer, M. Ortiz, "Data-driven computational mechanics", *Comput. Methods Appl. Mech. Eng.* **304** (2016), p. 81-101.
[17] R. Eggersmann, T. Kirchdoerfer, S. Reese, L. Stainier, M. Ortiz, "Model-Free Data-Driven inelasticity", *Comput. Methods Appl. Mech. Eng.* **350** (2019), p. 81-99.
[18] K. Karapiperis, L. Stainier, M. Ortiz, J. E. Andrade, "Data-Driven multiscale modeling in mechanics", *J. Mech. Phys. Solids* **147** (2021), article no. 104239.
[19] K. Karapiperis, M. Ortiz, J. E. Andrade, "Data-Driven nonlocal mechanics: Discovering the internal length scales of materials", *Comput. Methods Appl. Mech. Eng.* **386** (2021), article no. 114039.
[20] A. Mielke, "Evolution of rate-independent systems", in *Handbook of differential equations: Evolutionary equations. Vol. II*, vol. 2, Elsevier, 2005, p. 461-559.
[21] B. Halphen, Q. S. Nguyen, "Sur les matériaux standards généralisés", *J. Méc., Paris* **14** (1975), p. 39-63.
[22] H. Askes, M. A. Gutiérrez, "Implicit gradient elasticity", *Int. J. Numer. Methods Eng.* **67** (2006), no. 3, p. 400-416.
[23] F. Brezzi, "On the Existence, Uniqueness and Approximation of Saddle-Point Problems Arising from Lagrangian Multipliers", *Publications des séminaires de mathématiques et informatique de Rennes* (1974), no. S4, article no. 1.

[24] D. Kraft, "A software package for sequential quadratic programming", *DFVLR Forschungsber.* **28** (1988).
[25] N. Singh, C. V. Verhoosel, R. De Borst, E. H. Van Brummelen, "A fracture-controlled path-following technique for phase-field modeling of brittle fracture", *Finite Elem. Anal. Des.* **113** (2016), p. 14-29.